

A Diiron(I/II) μ -1,2-Carbonyl Complex Relevant to CO Binding on Fe(111)

Titto Sunil John,^{||} Devender Singh,^{||} Vincent Maurel,^{*} Ricardo García-Serres,^{*} and Leslie J. Murray^{*}



Cite This: *Inorg. Chem.* 2025, 64, 10488–10495



Read Online

ACCESS |



Metrics & More

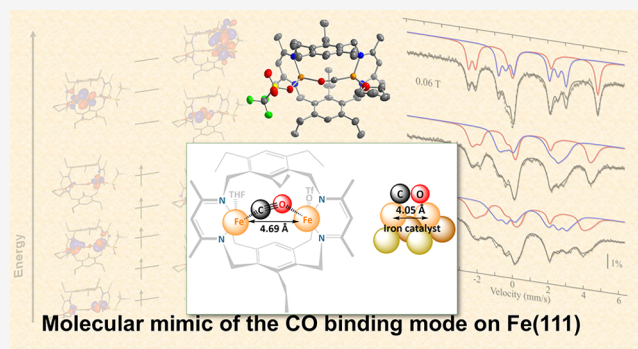


Article Recommendations



Supporting Information

ABSTRACT: Fischer–Tropsch conversion of syngas to hydrocarbons is proposed to begin with CO binding to the iron surface of the catalyst. CO adsorption on various iron facets of relevance to the Fischer–Tropsch process suggest that the Fe(111) surface is the most active for catalysis, and that CO bound to the penultimate layer of Fe atoms or the *b*-state is the resting state during catalysis. Notably, a μ -1,2 mode was discarded for the *b*-state due to a lack of exemplar molecular species and expectation that such a mode would have a higher energy infrared (IR) absorption than observed experimentally (viz. 1735–1860 cm^{-1}). Here, we report the synthesis of a diiron(I/II) complex in which CO binds μ -1,2: $(\text{Fe}(\text{OTf}))(\text{Fe}(\text{THF})(\mu$ -1,2-CO))L where L^{2-} is a bis(β -diketiminate) cyclophane (**1**). Surprisingly, the observed ν_{CO} at 1763 cm^{-1} for **1** compares well with that reported for *b*-state. Electron paramagnetic resonance (EPR), Mössbauer, and density functional theory (DFT) results support a weakly coupled $s = 3/2$ iron(I) and $s = 2$ iron(II) pair. Reduction of **1** results in C–O cleavage and C–C bond formation to yield a ketylidene (CCO) complex as a major product observed spectroscopically.



INTRODUCTION

Conversion of CO_2 and CO into long chain hydrocarbons is a key step in carbon-neutral fuel synthesis. The Fischer–Tropsch process converts CO and H_2 to hydrocarbons over a metal catalyst and was discovered in 1925. Although *in operando* techniques allow insight into the mechanism, there remain unanswered questions.¹ Here then, molecular species provide useful benchmarks to correlate structure with spectroscopic signatures. For example, proposed structures for how CO binds to the catalyst surfaces at different loadings have relied on molecular and heterogeneous precedent. Of the proposed mechanisms, the surface carbide mechanism is currently preferred. This mechanism begins with side-on CO adsorption to the metal surface followed by the CO bond cleavage to generate adsorbed C and O atoms, and is supported by experimental and computational studies on Fe(110) and Fe(100) surfaces that identify a transition state in which the CO molecular axis is parallel to the surface.^{2–9} Few investigations have explored the nature of CO binding and dissociation on Fe(111), despite the better catalytic performance of this surface over others.^{10–12} Seminal work by Seip et al. and Bartosch et al. on the CO adsorption on a Fe(111) surface observed three adsorbed-CO stretching modes (viz. *a*, *b*, *c* states), which are populated as a function of coverage and temperature.^{13,14} For the Fe(111) surface, the *b*-state is proposed as the state that evolves to CO bond cleavage under Fischer–Tropsch conditions, either by an equilibrium

with the *a*-state or directly, making the structural details of this state of import.¹³

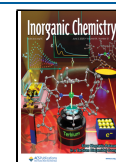
In those initial reports on the *b*-state, the structural assignment as being a CO terminally bound to the shallow hollow sites (tetrahedral holes) relied on two comparisons to precedent. First, the observed ν_{CO} is substantially lower in energy than expected for a μ -1,2 mode based on data reported for CO bound to the Ni(110) facet.^{13,15} Second, the 4.05 Å separation between Fe atoms in the on-top layer of the Fe(111) surface was greater than that for any reported polynuclear iron carbonyl complex. Specifically, molecular iron examples of CO ligands bound μ -1,2 or μ - η^1 : η^2 have Fe–Fe distances ≤ 4.0 Å. This proposed structure agrees with recent computational reports for the *b*-state, with a minor tilting away from normal to surface observed in some cases.¹⁶ Initial computational studies by Mehandru and Andersen using the atom superposition and electron delocalization molecular orbital (ASED-MO) level of theory, however, implicated the μ -1,2-CO binding across two iron atoms on the top layer and parallel to the metal surface as lowest in energy (Figure

Received: February 17, 2025

Revised: April 24, 2025

Accepted: May 12, 2025

Published: May 19, 2025



1).^{16–19} We surmise then that molecular precedent coupled with modern density functional theory (DFT) methods

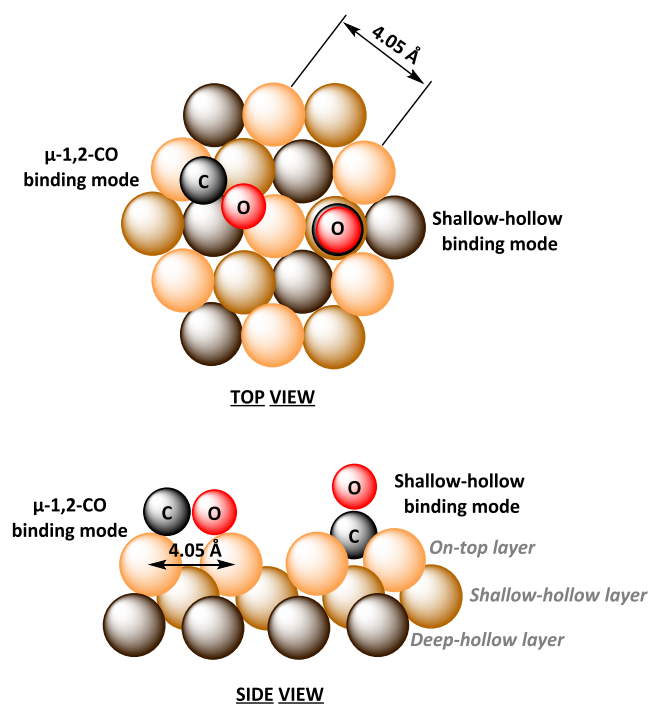


Figure 1. Proposed (shallow-hollow CO binding) and plausible (μ -1,2 CO binding) structures for *b*-state of CO binding on Fe(111) surface.

underpin the proposed structure of the *b*-state, in contrast to other Fe surfaces for which additional spectroscopic data have been reported.¹³

Previously, our group reported a di(μ -carbonyl)diiron(I) complex, $\text{Fe}_2(\mu\text{-CO})_2\text{L}$ ($\text{L}^{2-} = \text{bis}(\beta\text{-diketiminate})$ cyclophane) and a *cis*- μ -1,2-dinitrogen diiron complex, $(\text{FeBr})_2(\mu\text{-1,2-N}_2)\text{L}$ (Figure 2).^{20,21} For the former, serial reduction and silylation of this species effects the partial deoxygenative coupling of the CO ligands. Herein, we report the one-electron oxidation of $\text{Fe}_2(\mu\text{-CO})_2\text{L}$ to the diiron (I/II) complex $\text{Fe}_2(\mu\text{-CO})(\text{OTf})(\text{THF})\text{L}$, in which the CO coordinates in a μ -1,2 fashion and exhibits an IR absorption comparable to that reported for the CO bound *b*-state of the Fischer–Tropsch catalyst. Reduction of this compound results in CO homologation, suggesting that this mode is competent for CO bond scission.

EXPERIMENTAL AND COMPUTATIONAL SECTION

General Considerations. All manipulations were performed inside an Ar-filled Vigor glovebox unless otherwise stated. Tetrahydrofuran (THF) and *n*-hexane were purchased from Sigma-Aldrich. THF was dried using an Innovative Technologies solvent purification system (now Inert, Amesbury, MA). *n*-hexane was dried over NaK-benzophenone, heated to reflux, distilled and degassed. Solvents were stored over activated 3 Å molecular sieves (200 °C, < 20 mTorr) for at least 24 h prior to use. C_6D_6 was purchased from Cambridge Isotope Laboratories, dried over CaH_2 , heated to reflux, then distilled, degassed, transferred to the glovebox, and stored over activated 3 Å molecular sieves. Silver triflate (AgOTf) was purchased from Oakwood Chemical (Estill, SC). $\text{Fe}_2(\mu\text{-CO})_2\text{L}$ was prepared as reported.²⁰ ^1H Nuclear Magnetic Resonance (^1H NMR) spectra were recorded on a Bruker 400 MHz spectrometer equipped with a three-channel indirect detection probe with *z*-axis gradients. Chemical shifts are reported in δ (ppm) and referenced to solvent resonance at $\delta_{\text{H}} = 7.16$ ppm for benzene- d_6 . FT-IR spectra were collected on drop-casted samples using a ThermoFisher Scientific Nicolet iSS spectrometer equipped with an iD7 ATR stage, and using the OMNIC software package at 1.0 cm^{-1} resolution and 32 scans per sample.

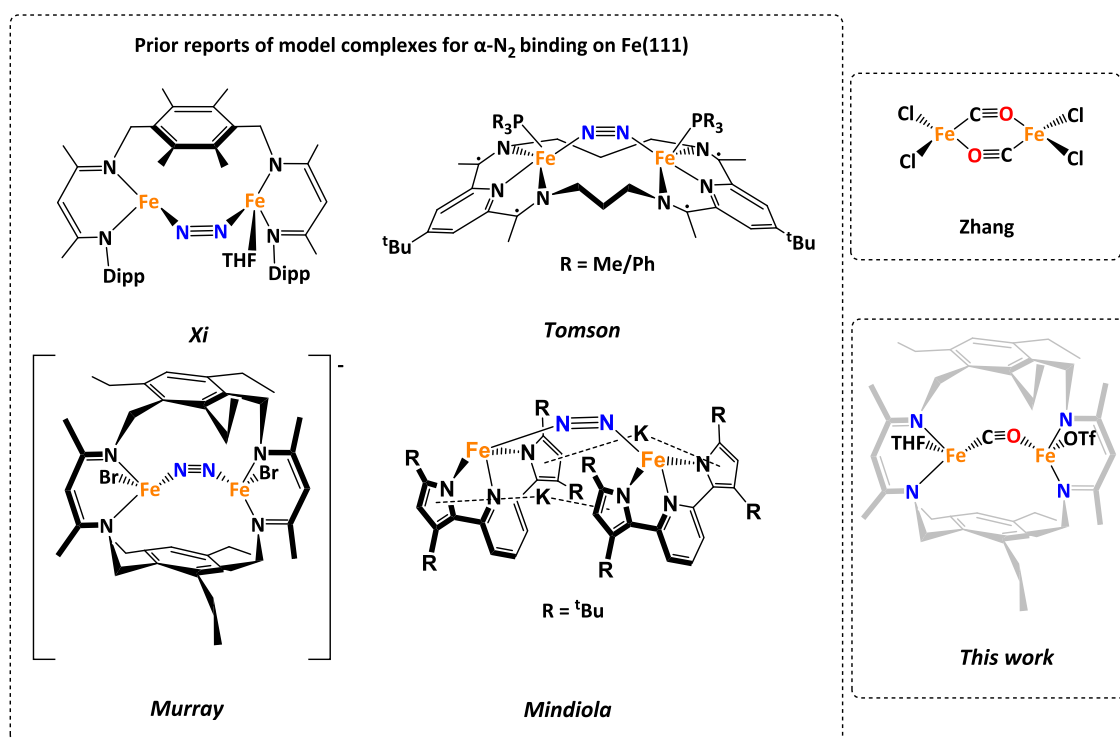
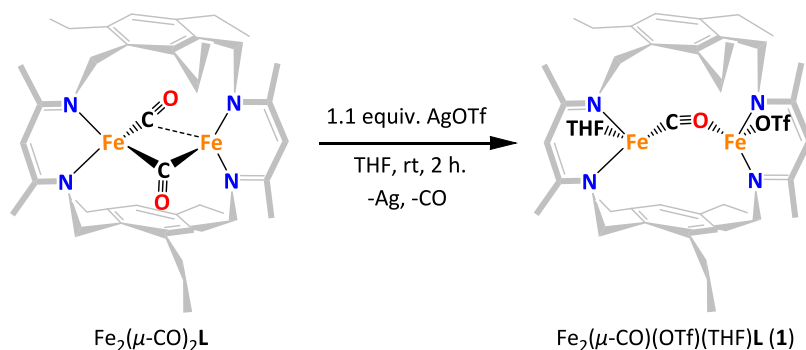


Figure 2. Model complexes for N_2 and CO adsorption on Fe(111) surface.

Scheme 1. Synthesis of the μ -1,2-Carbonyl Complex (1)

Synthetic Protocols. *Synthesis of $\text{Fe}_2(\mu\text{-CO})(\text{OTf})(\text{THF})\text{L}$ (1).* To a solution of $\text{Fe}_2(\mu\text{-CO})_2\text{L}$ (69.0 mg in 2 mL THF, 95.1 μmol) stirred with a Pyrex magnetic stir bar, silver triflate (26.85 mg, 104.5 μmol) was added. The reaction was stirred at ambient temperature for 2 h during which the reaction mixture gradually changed from dark yellow to greenish brown. After filtering the reaction mixture through Celite, which was pre-rinsed with anhydrous THF, the filtrate was layered with 1 mL hexane and stored at -33°C for 2 d to afford $\text{Fe}_2(\mu\text{-CO})(\text{OTf})(\text{THF})\text{L}$ as dark green powder (54.5 mg, 61.6%). Single crystals suitable for X-ray diffraction were grown from a solution of THF stored at -33°C . The ^{13}C -labeled isotopologue ($1\text{-}^{13}\text{CO}$) was synthesized following the above procedure using $\text{Fe}_2(\mu\text{-}^{13}\text{CO})_2\text{L}$ as the starting material. ^1H NMR (400 MHz, C_6D_6 , 298 K) δ (ppm): 182.93, 159.17, 46.36, 28.39, 10.93, 8.36, 3.83, 3.30, 1.56, 1.24, 0.89, 0.78, -3.64 , -6.24 , -7.12 , -13.86 , -28.85 , -30.28 , -81.59 , -118.30 , -130.78 . ATR-IR (cm^{-1}): 2959, 2926, 2871, 1763, 1521, 1457, 1430, 1392, 1373, 1326, 1233, 1205, 1171, 1021. Anal. Calc. for $\text{C}_{44}\text{H}_{64}\text{N}_4\text{O}_5\text{F}_3\text{S}_1\text{Fe}_2$ (%): C 56.84 H 6.94, N 6.03. Found: C 56.91, H 6.67, N 6.03.

Reduction of $\text{Fe}_2(\mu\text{-CO})(\text{OTf})(\text{THF})\text{L}$. $\text{Fe}_2(\mu\text{-CO})(\text{OTf})(\text{THF})\text{L}$ (9.8 mg, 11.5 μmol) was dissolved in PhMe and cooled to -33°C . To the thermally equilibrated solution, potassium graphite (KC_8) (2.0 mg, 15.0 μmol) was added. The reaction was stirred at -33°C for 2 d, warmed to ambient temperature, then filtered through Celite, which was pre-rinsed with PhMe, and solvent removed from the filtrate under reduced pressure. The residue was used as-obtained for spectroscopic measurements.

X-ray Crystallography. Low-temperature X-ray diffraction data for $\text{Fe}_2(\mu\text{-CO})(\text{OTf})(\text{THF})\text{L}$ (1) were collected on a Rigaku XtaLAB Synergy diffractometer coupled to a Rigaku Hypix detector with Cu $\text{K}\alpha$ radiation ($\lambda = 1.54184 \text{ \AA}$), from a PhotonJet microfocus X-ray source at 100 K. The diffraction images were processed and scaled using the CrysAlisPro software.²² The structure was solved through intrinsic phasing using SHELXT and refined against F2 on all data by full-matrix least-squares with SHELXL following established refinement strategies.^{23–25} All non-hydrogen atoms were refined anisotropically. All hydrogen atoms bound to carbon were included in the model at geometrically calculated positions and refined using a riding model. The isotropic displacement parameters of all hydrogen atoms were fixed to 1.2 times the U_{eq} value of the atoms to which they are linked (1.5 times for methyl groups). Details of the data quality and a summary of the residual values of the refinements are listed in Supporting Table 2.

Mössbauer Spectroscopy. The sample was ground into fine powder and placed in Delrin containers. Mössbauer spectra were measured on an Oxford Instruments Spectromag 4000 cryostat containing an 8 T split-pair superconducting magnet. The spectrometer was operated in constant acceleration mode in transmission geometry. The isomer shifts are referenced against a room temperature metallic iron foil. Analysis of the data was performed using the in-house developed Python package easyMoss.²⁶

Electron Paramagnetic Resonance Spectroscopy. EPR spectra were recorded using a Bruker EMX Plus spectrometer operating at X-band frequency with an ER 4122 SHQE Resonator

(perpendicular mode) and an Oxford Instruments ESR-900 flow cryostat. Powder samples were held in a gastight clear fused silica EPR sample holder (727-LPV-250 M from Wilmad), which was filled in gloves box under argon. Settings were kept constant for EPR measurements from 5 K up to 80 K: 9.399 GHz microwave frequency, 20 mW microwave power, 4 G modulation amplitude and 250s acquisition time.

Computational Methods. Electronic structure calculations were performed using the software package ORCA version 6.0.1. Optimized geometries were calculated using the TPSSh functional with the def2-TZVP(-f) basis set, Grimme's D4 dispersion correction and the preset conductor-like polarizable continuum model for THF (i.e., CPCM(THF)) as the solvent model.^{27–29} Single point, spin density, and vibrational frequency calculations performed on the optimized geometries included the zeroth order relativistic approximation with the functional and basis set used above.³⁰ The iso values for unrestricted natural orbitals (UNO) and spin density surfaces were set to maintain a 80.0 and 99.9% probability, respectively. Images were made using Gabedit 2.5.1.³¹ H atoms are omitted from the figures for clarity.

Mössbauer parameters were calculated using the method described by Neese and co-workers with an initial geometry optimization followed by the electron density calculation using the TPSS0 functional and the exact two-component Hamiltonian X2C for relativistic effects on all atoms and the modified aug-cc-pVTZ-J basis set on the Fe atoms.^{32–35}

RESULTS AND DISCUSSION

Reaction of $\text{Fe}_2(\mu\text{-CO})_2\text{L}$ with AgOTf in THF at ambient temperature affords a green species, 1, with one strong infrared vibration in the carbonyl region of the IR spectrum at 1763 cm^{-1} (Scheme 1 and Figure S2). From the absence of more than one absorption and the observed red-shift in the vibration relative to that in the starting complex (viz. 1801, 1846, and 1856 cm^{-1}), we inferred loss of one CO in 1 as oxidation would be expected to cause a hypsochromic shift for the CO stretching mode. The assignment of the band to a CO stretching mode was confirmed by using $\text{Fe}_2(\mu\text{-}^{13}\text{CO})_2\text{L}$ as the starting material to generate $1\text{-}^{13}\text{CO}$ for which the absorption at 1763 cm^{-1} in 1 redshifts to 1719 cm^{-1} ($\nu_{\text{calculated}} = 1723 \text{ cm}^{-1}$) (Figure S3). The frequency observed here is comparable to that observed for the lo-CO state for the CO inhibited form of the molybdenum-dependent nitrogenase cofactor ($\nu_{\text{CO}} = 1715 \text{ cm}^{-1}$), as well as that for the dicarbonyl complex $[\text{K}(\text{THF})_5][\text{Fe}_2(\text{CO})_2\text{L}]$ and the siloxycarbene complex $\text{Fe}_2(\mu\text{-}\eta^1\text{-}\eta^1\text{-CO})(\mu\text{-COSiMe}_3)\text{L}$ ($\nu_{\text{CO}} = 1809$ and 1700 , and 1741 cm^{-1} , respectively).^{20,36,37} From a combined DFT, applied-field Mössbauer, and EPR data on the dicarbonyl and siloxycarbene complexes, we concluded that both exhibit net ferromagnetic coupling through double-exchange, but the formal oxidation states of the two differ with dicarbonyl

described as a high-spin Fe^0 and low spin Fe^{I} pair, and the siloxycarbyne as an $S = 1 \text{ Fe}^{\text{II}}$ and $S = 1/2 \text{ Fe}^{\text{I}}$ pair. We noted the metal–ligand covalency and the Fisher-like character of the bridging siloxycarbyne complex, whereas no similar ligand is present in **1**, indicating a distinct electronic effect to activate the CO donor. The energy of the CO vibration in **1** is well within the range previously reported for the *b*-state for CO bound to the $\text{Fe}(111)$ surface.

Gratifyingly, the solid-state structure of **1** agrees with expectation from IR data of only one carbonyl ligand retained in the complex (Figure 3); however, this CO coordinates in a

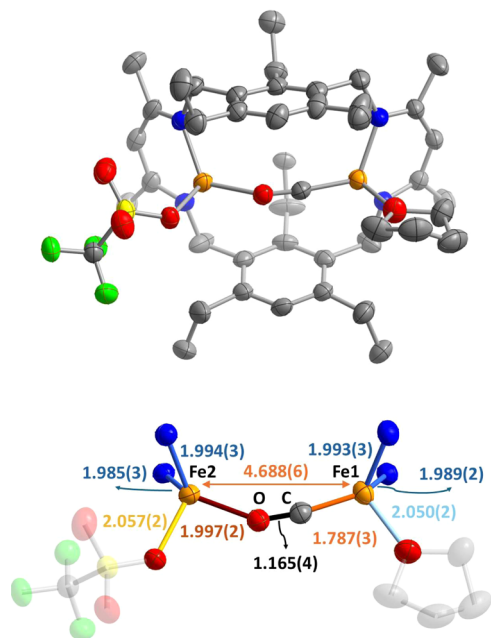


Figure 3. Solid state structure of **1** (top) and of the primary coordination spheres of the iron centers with pertinent bond lengths included (bottom). C, N, O, F, S and Fe atoms depicted as gray, dark blue, red, green and orange ellipsoids at 50% probability, respectively. The OTf and one ethyl arm were positionally disordered with the higher occupancy model depicted. All H atoms and solvent molecules are removed for clarity.

μ -1,2 fashion rather than a μ - η^1 : η^1 mode. Refinement affords the best model with the C and O atoms of the CO ligand bound to Fe1 and Fe2, respectively. Bond valence sum analysis supports formal charges for Fe1 and Fe2 as 1.27 and 2.03, respectively.³⁸ Moreover, the supporting ligands of THF bound to Fe1 and OTf to Fe2 with the $\text{Fe1-C}\equiv\text{O-Fe2}$ bond angles (e.g., $\angle\text{Fe1-C-O}$ angle of $171.752(3)^\circ$) are consistent with the formal oxidation state assignments (Table S1).^{39–46} Each Fe center in **1** is in a pseudotetrahedral environment with τ_4 values of 0.85 and 0.83 for Fe1 and Fe2, respectively.⁴⁷ The Fe–Fe distance of $4.6886(7) \text{ \AA}$ observed here is longer than that for $(\text{FeCl}_2)_2(\mu$ -1,2-CO)₂ (viz. 3.958 \AA)—the only prior example of a diiron complex with one or more μ -1,2 carbonyl donors—and comparable to that in the diiron μ -1,2- N_2 model complexes proposed as models for side-on α - N_2 binding to the $\text{Fe}(111)$ surface (viz. 4.857 , 4.563 , 4.783 and 4.673 \AA) (Figure 2).^{21,48–51} For $(\text{FeCl}_2)_2(\mu$ -1,2-CO)₂, Zhang and co-workers reported the two CO ligands are adopting *cis*- μ -1,2 modes with the CO stretching mode observed in IR spectra at 1938 cm^{-1} and relatively long Fe–C and Fe–O distances of $2.179(1)$ and $2.190(1) \text{ \AA}$,

respectively, all of which agree with the formal iron(II) oxidation states. The coordination of C to Fe(I) and O to Fe(II) is consistent with what is observed for the family of crystallographically characterized μ -1,2-carbonyl complexes where the C atom is bound to the electron rich metal ion and O atom to the electrophilic metal atom,^{52–56} and also bears similarity to the push–pull electronic effect for activation of small molecules.⁵⁷ Contrary to the ligand field on each Fe atom in **1**, the few structurally validated homometallic dinuclear examples either have each metal center coordinated within disparate ligand fields or both metal ions are bound to strong field ancillary donors.^{39–45,58} Notably, all except one of the reported homometallic dinuclear examples feature early 3d transition metals,^{39–45,58} with the exception being the aforementioned $(\text{FeCl}_2)_2(\mu$ -1,2-CO)₂.⁴⁸

Zero-field Mössbauer measurements recorded on a solid sample of **1** at 20, 31 and 80 K showed two distinct quadrupole doublets with different rates of broadening with decreasing temperature (Figure 4), which enables peak assignment in a

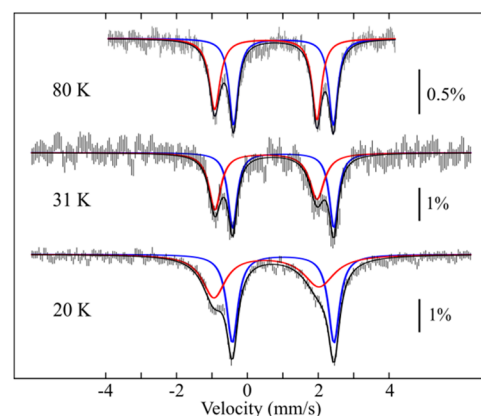


Figure 4. Zero-field Mössbauer spectra of **1** recorded at 80, 31 and 20 K (top to bottom). Red and blue solid lines are the individual quadrupole doublet simulations, and the black solid lines are the composite simulated spectra. Based on the isomer shifts, the blue component is assigned to HS Fe^{II} , while the red component is assigned to $S = 3/2 \text{ Fe}^{\text{I}}$. Fitting parameters are given in Tables S4 and S5.

non-nested (intercalated) fashion. The Mössbauer parameters at 80 K are $\delta/\Delta_{\text{EQ}}$ (mm/s) = $1.02/2.82$ and $0.52/2.89$, indicating valence localized, locally high spin $s = 2 \text{ Fe(II)}$ and $s = 3/2 \text{ Fe(I)}$ centers, respectively, consistent with DFT calculations (vide infra).⁵⁹ In addition, solution magnetic moment measured at $23 \text{ }^\circ\text{C}$ using Evan's method ($\mu_{\text{eff}} = 6.53 \mu_{\text{B}}$) agrees with weak ferromagnetic coupling as the observed moment is comparable to that for uncoupled Fe centers (viz., $6.25 \mu_{\text{B}}$).⁶⁰ In contrast to the previously reported ferromagnetic $S = 7/2 \mu$ -1,2 N_2 complex which exhibits valence delocalization between the Fe centers, the localized Fe centers in **1** suggested a different picture of magnetic coupling between the two Fe centers. Seeking to understand the nature of ground state magnetic interaction, field-applied Mössbauer spectrum of **1** was measured. The spectra measured at 5.8 and 2.3 K in a 0.06 T applied magnetic field are nearly identical, allowing for accurate spin-Hamiltonian simulation in the slow-relaxation limit. The simulations assuming either two uncoupled ions ($s = 3/2 \text{ Fe(I)}$ and $s = 2 \text{ Fe(II)}$) or a weak ferromagnetic interaction resulting in $S = 7/2$ ground state, yielded equally good fits, demanding additional data to support one or the

other model of the electronic structure (Figure S4). Solid-state X-band EPR spectra on the sample used for Mössbauer measurements were obtained at temperatures ranging from 5 to 80 K. At 5 K, a strong signal is observed at low magnetic field, which intersects the baseline close to 500 G or $g \sim 13.9$ and is close to that expected for the lowest field $m_S = -7/2$ to $+7/2$ transition of a $S = 7/2$ system with ratio $E/D = 0.26$ (Figure S6). At higher temperatures, this feature decreases concomitant with the appearance of broad features at higher magnetic fields, with the latter becoming the main features at and above 30 K. Although these new features cannot be assigned unequivocally, these are observed at magnetic field values comparable to those expected for the $m_S = -5/2$ to $+5/2$ transition of a $S = 7/2$ system with ratio $E/D = 0.26$ for which higher field transitions at $g = 8.9, 2.7,$ and 1.9 are expected as the higher energy m_S states are populated. This temperature dependence is consistent with a D value of ~ -6 cm^{-1} , since the energy levels of $m_S = \pm 5/2$ states are expected to be higher than the energy levels of $m_S = \pm 7/2$ states by a quantity of $4D$.

The bridging mode and the differences in oxidation state are reminiscent of push–pull complexes in which a diatomic ligand bridges a Lewis acidic metal and an electron-rich metal ion capable of π -backbonding into the bridging ligand. To estimate the extent of activation expected in the absence of the Fe(II) center, we searched for an analogous three-coordinate monocarbonyl complex supported by weak-field donors. A previously reported terminal monocarbonyl complex with high spin ($S = 3/2$) Fe(I), $[\text{Fe}(\text{CO})(\text{HMDS})_2]^-$ (where HMDS^- = hexamethyldisilazide) with $\nu_{\text{CO}} = 1822$ cm^{-1} is the only reasonable comparison; we note, however, that the β -diketiminato donors in **1** are less π -basic and σ -donating than amides ligands and the extent of π donation is also influenced by the N–Fe–N bond angles among other structural parameters in both complexes. With that caveat then, comparison to our value provides an estimate of ~ 60 cm^{-1} for the enhanced activation afforded by the Lewis acidity of Fe2.^{61,62} This value is comparable to that computationally predicted for N_2 by the side-on Co(I) in the trinuclear $\text{Co}_3\text{N}_2\text{L}^{\text{Et/Me}}$, but notably less than the 134 cm^{-1} decrease observed for $(\text{depe})_2\text{Fe}^0\text{--N}\equiv\text{N--Fe}^{2+}(\text{Tp}^i\text{Pr}_2)$ complex vs $(\text{depe})_2\text{Fe}^0\text{--N}_2$.^{62,63} The mixed valence and the push–pull contribution in **1** evoke the resonating valence band model proposed for CO activation on a metal surface.⁶⁴

The preference for the ferromagnetically coupled Fe atoms in the ground state for **1** contrasts the antiferromagnetic coupling in the parent complex $\text{Fe}_2(\mu\text{-CO})_2\text{L}$ ($S = 0$). As noted previously, the local spin states and the coupling schemes between iron centers vary substantially for complexes of this ligand, being sensitive to reduction and silylation as in the previously reported series of complexes in the conversion of $\text{Fe}_2(\text{CO})_2\text{L}$ to $\text{Fe}_2(\text{CCO})\text{L}$.²⁰ Also, the large metal–metal separation in **1** of $4.68(9)$ Å as compared to those of less than 2.6 Å in the dicarbonyl to ketenylidene series of complexes precludes a double exchange mechanism through direct metal–metal bonding to stabilize the $S = 7/2$ ground state.^{65–67} Taken together, **1** and the prior CO homologation report demonstrate the diverse electronic and geometric changes accessible to polynuclear metal complexes coordinated to weak field donors (here, BDIs) and even for the same ligand as a function or formal oxidation state and the identity of bridging ligands.

We then employed DFT methods to gain insight into the electronic structure of complex **1**. DFT calculations performed on the X-ray diffraction modeled atomic coordinates of **1** using the TPSSh functional, Alrichs' def2-tzvp(-f) basis set, ZORA, and Grimme's D4 dispersion correction for the high spin $S = 7/2$ state and the ferromagnetically coupled Broken Symmetry state with $M_S = 1/2$ support the $S = 7/2$ as the electronic ground state, in agreement with Mössbauer and EPR measurements.^{27–29} The calculated C–O stretching frequency of 1775 cm^{-1} agrees well with the measured value of 1763 cm^{-1} (Figure S7). Similar to the isoelectronic *cis*-(μ -1,2- N_2) complex, the seven singly occupied orbitals are predominantly Fe $3d$ in character, which is also reflected in the spin density plot (Figures 5 and S9).²¹ To gauge the extent of charge

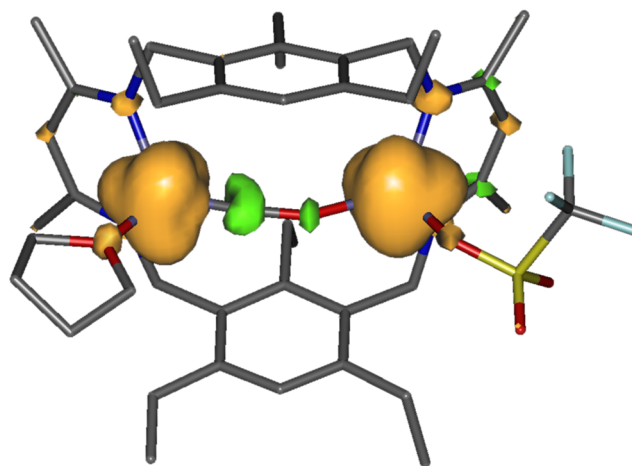
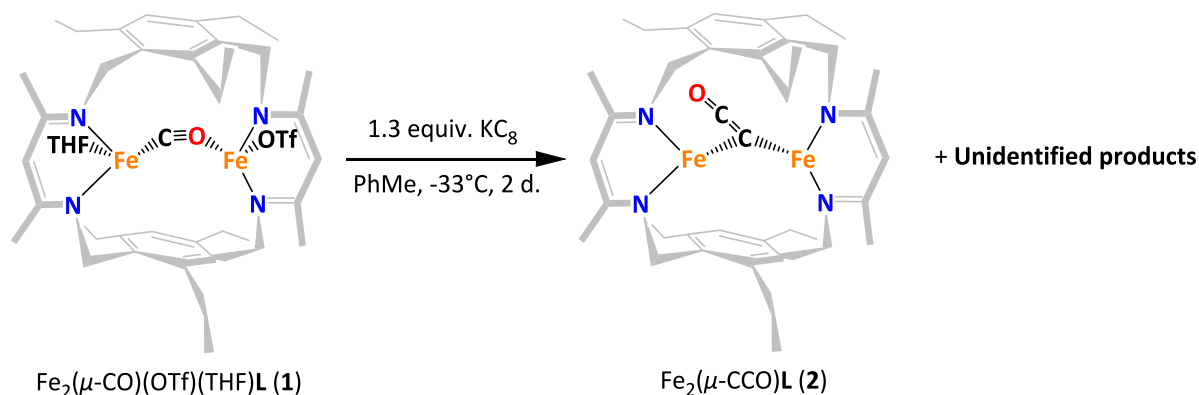


Figure 5. Spin density surface plot for **1** at 99.9% isosurface for the $S = 7/2$ state calculated using TPSSh functional, the def2-tzvp(-f) basis set with ZORA and Grimme's D4 correction showing that the majority of the α density (gold) is localized on the two Fe atoms with a minor β density (green) contribution on the μ -1,2-CO ligand.

transfer from the iron(I) (or Fe1) to the iron(II) (or Fe2) center, we also calculated a hypothetical heteronuclear FeZn analog of **1** in which Fe2 is replaced by Zn(II). Using the Mulliken spin populations as an approximate reporter, we observed a minor increase in the population at Fe1 in the heteronuclear complex versus **1**, consistent with the weak ferromagnetic coupling between the two centers. Attempts to estimate the double exchange parameter, B , from the calculations yielded an unreasonably large value ($B > 5000$ cm^{-1}), analogous to previous observations for other diiron complexes, and prevent meaningful computationally derived values for the energy separation between states in terms of B and J values.^{20,68} In agreement with the extent of CO activation observed from IR and X-ray diffraction data, the calculated Löwdin C–O bond order is 2.48 and the two highest doubly occupied frontier orbitals are metal to ligand π backbonding in character from Fe $3d_{\pi}$ to CO π^* . The calculated Mössbauer parameters using the method described by Neese and co-workers, with the TPSS0 functional, the exact two-component Hamiltonian X2C for relativistic effects, and the modified aug-cc-pVTZ-J on the Fe atoms only, are isomer shifts of 0.52 and 0.91 mm/s, and quadrupole splittings of 3.04 and 2.89 mm/s, for Fe1 and Fe2, respectively, and are in excellent agreement with the observed values (vide supra).³²

We reasoned that the significant CO π^* parentage of the LUMO and LUMO + 1 implied that potential for further CO

Scheme 2. Reduction of the μ -1,2-Carbonyl Complex (1)

activation upon reduction of the complex. To our surprise, however, reaction of 1 equiv KC_8 with **1** afforded $Fe_2(\mu-CCO)L$ (**2**) as the major species based on 1H NMR spectroscopy (Scheme 2, Figure S10 and S11). We previously reported **2** as the product from serial reduction and silylation of $Fe_2(\mu-CO)_2L$.²⁰ Although a detailed mechanistic study is required, prior reports of CO ligand conversion to ketenylidenes in metal complexes are typically proposed from CO migration to a carbide ligand.^{69,70} Then, a similar mechanism in which CO bond scission upon reduction of **1** leads to a transient carbide-bridged diiron species, followed by CO transfer from unreacted **1** seems plausible. The mechanism is likely more complex as an O atom acceptor is also required, but the possible formation of a transient iron carbide species evokes the carburization of the Fe catalyst in the Fischer–Tropsch process.² Recently, Smith and co-workers proposed a transient iron carbide arising from $C\equiv P^-$ cleavage, which rapidly dimerizes to the corresponding ethynediyl complex.⁷¹

CONCLUSIONS

The diiron μ -1,2 bound carbonyl complex, **1**, demonstrates the capacity for CO to bind across Fe atoms separated by distances as large as 4.6 Å. Complex **1** exhibits a CO stretching frequency of 1763 cm^{-1} , in range for what is observed for *b*-state for CO bound to the Fe(111) surface, suggesting that such CO coordination modes are reasonable for surface Fe atoms. With respect to the *b*-state of CO coordination on Fe(111) then, the diiron μ -1,2 bound carbonyl complex, **1**, suggests that more surface spectroscopic measurements may be needed to refine the structural assignment. Formation of the $Fe_2(\mu-CCO)L$ (**2**) upon reduction of **1** highlights the potential for simple polynuclear metal complexes, such as **1**, to mirror Fischer–Tropsch like reactivity of metal surfaces. Mechanistic studies on the pathway for CO scission starting from **1** and the possible transient species generated are of ongoing interest.

ASSOCIATED CONTENT

Supporting Information

The Supporting Information is available free of charge at <https://pubs.acs.org/doi/10.1021/acs.inorgchem.5c00759>.

Spectroscopic; Mossbauer fitting; and crystallographic data (PDF)

Accession Codes

Deposition Number 2416731 contains the supplementary crystallographic data for this paper. These data can be obtained free of charge via the joint Cambridge Crystallographic Data

Centre (CCDC) and Fachinformationszentrum Karlsruhe Access Structures service.

AUTHOR INFORMATION

Corresponding Authors

Vincent Maurel – Université Grenoble Alpes, CEA, CNRS, IRIG, SyMMES, Grenoble 38000, France; orcid.org/0000-0002-0855-6412; Email: vincent.maurel@cea.fr

Ricardo García-Serres – Univ. Grenoble Alpes, CNRS, CEA, IRIG, Laboratoire de Chimie et Biologie des Métaux, Grenoble 38000, France; orcid.org/0000-0001-5203-0568; Email: ricardo.garcia@cea.fr

Leslie J. Murray – Center for Catalysis and Florida Center for Heterocyclic Chemistry, Department of Chemistry, University of Florida, Gainesville, Florida 32611, United States; orcid.org/0000-0002-1568-958X; Email: murray@chem.ufl.edu

Authors

Titto Sunil John – Center for Catalysis and Florida Center for Heterocyclic Chemistry, Department of Chemistry, University of Florida, Gainesville, Florida 32611, United States; orcid.org/0000-0002-6100-4262

Devender Singh – Center for Catalysis and Florida Center for Heterocyclic Chemistry, Department of Chemistry, University of Florida, Gainesville, Florida 32611, United States

Complete contact information is available at:

<https://pubs.acs.org/10.1021/acs.inorgchem.5c00759>

Author Contributions

^{||}T.S.J. and D.S. contributed equally to this work. The manuscript was written through contributions of all authors. All authors have given approval to the final version of the manuscript.

Funding

T.S.J., D.S., and L.J.M. thank the National Institutes of Health (R01-GM123241) and the National Science Foundation (CHE-2102098) for funding. R.G.S. thanks Labex ARCANE, ANR-17-EURE-0003, for funding. V.M. thanks IR INFRANALYTICS FR2054 for financial support for conducting the EPR experiments.

Notes

The authors declare no competing financial interest.

ACKNOWLEDGMENTS

T.S.J., D.S., and L.J.M. thank Dr S. MacMillan for X-ray diffraction measurements.

REFERENCES

- (1) Anderson, R. B. *Fischer–Tropsch Synthesis*; U.S. Department of Energy Office of Scientific and Technical Information, 1984.
- (2) De Smit, E.; Weckhuysen, B. M. The Renaissance of Iron-Based Fischer–Tropsch Synthesis: On the Multifaceted Catalyst Deactivation Behaviour. *Chem. Soc. Rev.* **2008**, *37* (12), 2758–2781.
- (3) Stibor, A.; Kresse, G.; Eichler, A.; Hafner, J. Density Functional Study of the Adsorption of CO on Fe(). *Surf. Sci.* **2002**, *507*–*510*, 99–102.
- (4) Moon, D. W.; Cameron, S.; Zaera, F.; Eberhardt, W.; Carr, R.; Bernasek, S. L.; Gland, J. L.; Dwyer, D. J. A Tilted Precursor for CO Dissociation on the Fe(100) Surface. *Surf. Sci.* **1987**, *180* (1), L123–L128.
- (5) Nassir, M. H.; Frühberger, B.; Dwyer, D. J. Coverage Dependence of CO Dissociation on Clean and Hydrogen Presaturated Fe(100) Surface. *Surf. Sci.* **1994**, *312* (1), 115–123.
- (6) Jiang, D. E.; Carter, E. A. Adsorption and Dissociation of CO on Fe(1 1 0) from First Principles. *Surf. Sci.* **2004**, *570* (3), 167–177.
- (7) Gonzalez, L.; Miranda, R.; Ferrer, S. A Thermal Desorption Study of the Adsorption of CO on Fe(110); Enhancement of Dissociation by Surface Defects. *Surf. Sci.* **1982**, *119* (1), 61–70.
- (8) Erley, W. Vibrational Spectra of CO Chemisorbed on Fe (110). *J. Vac. Sci. Technol.* **1981**, *18* (2), 472–475.
- (9) Wedler, G.; Ruhmann, H. Laser Induced Thermal Desorption of Carbon Monoxide from Fe(110) Surfaces. *Surf. Sci.* **1982**, *121* (3), 464–486.
- (10) Spencer, N. D.; Schoonmaker, R. C.; Somorjai, G. A. Iron Single Crystals as Ammonia Synthesis Catalysts: Effect of Surface Structure on Catalyst Activity. *J. Catal.* **1982**, *74* (1), 129–135.
- (11) Davies, R.; Edwards, D.; Gräfe, J.; Gilbert, L.; Davies, P.; Hutchings, G.; Bowker, M. The Oxidation of Fe(111). *Surf. Sci.* **2011**, *605* (17), 1754–1762.
- (12) Chen, J.; Chen, Y.; Wang, H.; Hu, P. Correlation between the Structural Features and Intrinsic Activity Trend of Fe Surfaces for Ammonia Synthesis. *Catal. Sci. Technol.* **2023**, *13* (18), 5237–5247.
- (13) Bartosch, C. E.; Whitman, L. J.; Ho, W. The Adsorption, Interconversion, and Dissociation of CO on Fe(111). *J. Chem. Phys.* **1986**, *85* (2), 1052–1060.
- (14) Seip, U.; Tsai, M.-C.; Christmann, K.; Küppers, J.; Ertl, G. Interaction of Co with an Fe(111) Surface. *Surf. Sci.* **1984**, *139* (1), 29–42.
- (15) Ertl, G. Primary Steps in Catalytic Synthesis of Ammonia. *J. Vac. Sci. Technol., A* **1983**, *1* (2), 1247–1253.
- (16) Booyens, S.; Bowker, M.; Willock, D. J. The Adsorption and Dissociation of CO on Fe(111). *Surf. Sci.* **2014**, *625*, 69–83.
- (17) Mehandru, S. P.; Anderson, A. B. Binding and Orientations of CO on Fe(110), (100), and (111): A Surface Structure Effect from Molecular Orbital Theory. *Surf. Sci.* **1988**, *201* (1), 345–360.
- (18) Chen, Y.-H.; Cao, D.-B.; Jun, Y.; Li, Y.-W.; Wang, J.; Jiao, H. Density Functional Theory Study of CO Adsorption on the Fe(1 1 1) Surface. *Chem. Phys. Lett.* **2004**, *400* (1), 35–41.
- (19) Huo, C.-F.; Ren, J.; Li, Y.-W.; Wang, J.; Jiao, H. CO Dissociation on Clean and Hydrogen Precovered Fe(111) Surfaces. *J. Catal.* **2007**, *249* (2), 174–184.
- (20) Singh, D.; Knight, B. J.; Catalano, V. J.; García-Serres, R.; Maurel, V.; Mouesca, J.-M.; Murray, L. J. Partial Deoxygenative CO Homocoupling by a Diiron Complex. *Angew. Chem., Int. Ed.* **2023**, *62* (41), No. e202308813.
- (21) Torres, J. F.; Oi, C. H.; Moseley, I. P.; El-Sakkout, N.; Knight, B. J.; Shearer, J.; García-Serres, R.; Zadrozny, J. M.; Murray, L. J. Dinitrogen Coordination to a High-Spin Diiron(I/II) Species. *Angew. Chem., Int. Ed.* **2022**, *61* (22), No. e202202329.
- (22) *CrysAlisPro*; Rigaku OD: The Woodlands, TX, 2015.
- (23) Sheldrick, G. M. A Short History of SHELX. *Acta Crystallogr., Sect. A: Found. Crystallogr.* **2008**, *64* (1), 112–122.
- (24) Sheldrick, G. M. SHELXT – Integrated Space-Group and Crystal-Structure Determination. *Acta Crystallogr., Sect. A: Found. Adv.* **2015**, *71* (1), 3–8.
- (25) Müller, P. Practical Suggestions for Better Crystal Structures. *Crystallogr. Rev.* **2009**, *15* (1), 57–83.
- (26) Garcia-Serres, R. easyMoss: A Python/PyQt5 User-Friendly Application for the Simulation of Mössbauer Spectra. 2021 DOI: 10.5281/zenodo.5634948.
- (27) Caldeweyher, E.; Bannwarth, C.; Grimme, S. Extension of the D3 Dispersion Coefficient Model. *J. Chem. Phys.* **2017**, *147* (3), No. 034112.
- (28) Tao, J.; Perdew, J. P.; Staroverov, V. N.; Scuseria, G. E. Climbing the Density Functional Ladder: Nonempirical Meta-Generalized Gradient Approximation Designed for Molecules and Solids. *Phys. Rev. Lett.* **2003**, *91* (14), No. 146401.
- (29) Staroverov, V. N.; Scuseria, G. E.; Tao, J.; Perdew, J. P. Comparative Assessment of a New Nonempirical Density Functional: Molecules and Hydrogen-Bonded Complexes. *J. Chem. Phys.* **2003**, *119* (23), 12129–12137.
- (30) van Lenthe, E.; Ehlers, A.; Baerends, E.-J. Geometry Optimizations in the Zero Order Regular Approximation for Relativistic Effects. *J. Chem. Phys.* **1999**, *110* (18), 8943–8953.
- (31) Allouche, A.-R. Gabedit—A Graphical User Interface for Computational Chemistry Softwares. *J. Comput. Chem.* **2011**, *32* (1), 174–182.
- (32) Santra, G.; Neese, F.; Pantazis, D. A. Extensive Reference Set and Refined Computational Protocol for Calculations of 57Fe Mössbauer Parameters. *Phys. Chem. Chem. Phys.* **2024**, *26* (35), 23322–23334.
- (33) Grimme, S. Accurate Calculation of the Heats of Formation for Large Main Group Compounds with Spin-Component Scaled MP2 Methods. *J. Phys. Chem. A* **2005**, *109* (13), 3067–3077.
- (34) Liu, W.; Peng, D. Exact Two-Component Hamiltonians Revisited. *J. Chem. Phys.* **2009**, *131* (3), No. 031104.
- (35) Hedegård, E. D.; Kongsted, J.; Sauer, S. P. A. Optimized Basis Sets for Calculation of Electron Paramagnetic Resonance Hyperfine Coupling Constants: Aug-Cc-pVTZ-J for the 3d Atoms Sc–Zn. *J. Chem. Theory Comput.* **2011**, *7* (12), 4077–4087.
- (36) Spatzal, T.; Perez, K. A.; Einsle, O.; Howard, J. B.; Rees, D. C. Ligand Binding to the FeMo-Cofactor: Structures of CO-Bound and Reactivated Nitrogenase. *Science* **2014**, *345* (6204), 1620–1623.
- (37) Van Stappen, C.; Decamps, L.; Cutsail, G. E.; Björnsson, R.; Henthorn, J. T.; Birrell, J. A.; Debeer, S. The Spectroscopy of Nitrogenases. *Chem. Rev.* **2020**, *120* (12), 5005–5081.
- (38) Zheng, H.; Langner, K. M.; Shields, G. P.; Hou, J.; Kowiel, M.; Allen, F. H.; Murshudov, G.; Minor, W. Data Mining of Iron(II) and Iron(III) Bond-Valence Parameters, and Their Relevance for Macromolecular Crystallography. *Acta Cryst. D* **2017**, *73* (4), 316–325.
- (39) Monillas, W. H.; Yap, G. P. A.; MacAdams, L. A.; Theopold, K. H. Binding and Activation of Small Molecules by Three-Coordinate Cr(I). *J. Am. Chem. Soc.* **2007**, *129* (26), 8090–8091.
- (40) Akturk, E. S.; Yap, G. P. A.; Theopold, K. H. Mechanism-Based Design of Labile Precursors for Chromium(I) Chemistry. *Chem. Commun.* **2015**, *51* (84), 15402–15405.
- (41) Schneider, M.; Weiss, E. Kristall- und molekülstruktur von tetrakis(tetrahydrofuran)vanadium(II)-bis[hexacarbonylvanadat(–I)], ein beispiel für eine lineare carbonylbrücke. *J. Organomet. Chem.* **1976**, *121* (3), 365–371.
- (42) Wang, W.; Li, J.; Yin, L.; Zhao, Y.; Ouyang, Z.; Wang, X.; Wang, Z.; Song, Y.; Power, P. P. Half-Sandwich Metal Carbonyl Complexes as Precursors to Functional Materials: From a Near-Infrared-Absorbing Dye to a Single-Molecule Magnet. *J. Am. Chem. Soc.* **2017**, *139* (34), 12069–12075.
- (43) Kong, G.; Harakas, G. N.; Whittlesey, B. R. An Unusual Transition Metal Cluster Containing a Seven Metal Atom Plane. Syntheses and Crystal Structures of [Mn][Mn7(THF)6(CO)12]2,

- Mn₃(THF)₂(CO)₁₀, and [Mn(THF)₆][Mn(CO)₅]₂. *J. Am. Chem. Soc.* **1995**, *117* (12), 3502–3509.
- (44) Osborne, J. H.; Rheingold, A. L.; Trogler, W. C. Synthesis, Structure, and Electronic Properties of (η⁵-C₅Me₅)₂V(μ₂-OC)V(CO)₅. A Complex with a Linear Vanadium–Oxygen–Carbon–Vanadium Bond. *J. Am. Chem. Soc.* **1985**, *107* (22), 6292–6297.
- (45) Vrtis, R. N.; Bott, S. G.; Lippard, S. J. Linear Carbonyl-Bridged, Dinuclear Tantalum Siloxycarbyne Complexes. *Organometallics* **1992**, *11* (1), 270–277.
- (46) Fritz, M.; Demeshko, S.; Würtele, C.; Finger, M.; Schneider, S. Linearly Bridging N₂ versus CO: Chemical Bonding and Spin-Controlled Reactivity. *Eur. J. Inorg. Chem.* **2023**, *26* (11), No. e202300011.
- (47) Yang, L.; R Powell, D.; P Houser, R. Structural Variation in Copper(i) Complexes with Pyridylmethylamide Ligands: Structural Analysis with a New Four-Coordinate Geometry Index, τ₄. *Dalton Trans.* **2007**, *0* (9), 955–964.
- (48) Zhang, Z.-Z.; Zhang, J.-K.; Zhang, W.-D.; Xi, H.-P.; Cheng, H.; Wang, H.-G. Carbonylation of Iron(II) Halide in the Presence of Chelate Diphosphine Ligands. Molecular Structure of a Novel Intermolecular Adduct [FeC₁₂(Dppe)₂][Fe₂(CO)₂Cl₄]. *J. Organomet. Chem.* **1996**, *515* (1), 1–9.
- (49) Liu, T.; Gau, M. R.; Tomson, N. C. Mimicking the Constrained Geometry of a Nitrogen-Fixation Intermediate. *J. Am. Chem. Soc.* **2020**, *142* (18), 8142–8146.
- (50) Sorsche, D.; Miehl, M. E.; Searles, K.; Gouget, G.; Zolnhofer, E. M.; Fortier, S.; Chen, C.-H.; Gau, M.; Carroll, P. J.; Murray, C. B.; Caulton, K. G.; Khusniyarov, M. M.; Meyer, K.; Mendiola, D. J. Unusual Dinitrogen Binding and Electron Storage in Dinuclear Iron Complexes. *J. Am. Chem. Soc.* **2020**, *142* (18), 8147–8159.
- (51) Feng, R.; Jiang, Y.; Shi, X.; Wang, X.; Chen, W.; Xie, F.; Su, J.; Wei, J.; Ye, S.; Xi, Z. One-Electron Reduction of Constrained and Unsymmetric Diiron Dinitrogen Complexes. *CCS Chem.* **2023**, *5* (11), 2473–2481.
- (52) Osipova, E. S.; Sedlova, D. V.; Gutsul, E. I.; Nelyubina, Y. V.; Dorovatovskii, P. V.; Epstein, L. M.; Filippov, O. A.; Shubina, E. S.; Belkova, N. V. Reactivity of Heterobimetallic Ion Pairs in Formic Acid Dehydrogenation. *Organometallics* **2023**, *42* (18), 2651–2660.
- (53) Osipova, E. S.; Gulyaeva, E. S.; Gutsul, E. I.; Kirikina, V. A.; Pavlov, A. A.; Nelyubina, Y. V.; Rossin, A.; Peruzzini, M.; Epstein, L. M.; Belkova, N. V.; Filippov, O. A.; Shubina, E. S. Bifunctional Activation of Amine-Boranes by the W/Pd Bimetallic Analogs of “Frustrated Lewis Pairs”. *Chem. Sci.* **2021**, *12* (10), 3682–3692.
- (54) Pappas, I.; Chirik, P. J. Catalytic Proton Coupled Electron Transfer from Metal Hydrides to Titanocene Amides, Hydrazides and Imides: Determination of Thermodynamic Parameters Relevant to Nitrogen Fixation. *J. Am. Chem. Soc.* **2016**, *138* (40), 13379–13389.
- (55) Mazzacano, T. J.; Leon, N. J.; Waldhart, G. W.; Mankad, N. P. Fundamental Organometallic Chemistry under Bimetallic Influence: Driving β-Hydride Elimination and Diverting Migratory Insertion at Cu and Ni. *Dalton Trans.* **2017**, *46* (17), 5518–5521.
- (56) Levina, V. A.; Rossin, A.; Belkova, N. V.; Chierotti, M. R.; Epstein, L. M.; Filippov, O. A.; Gobetto, R.; Gonsalvi, L.; Lledós, A.; Shubina, E. S.; Zanobini, F.; Peruzzini, M. Acid–Base Interaction between Transition-Metal Hydrides: Dihydrogen Bonding and Dihydrogen Evolution. *Angew. Chem.* **2011**, *123* (6), 1403–1406.
- (57) Geri, J. B.; Shanahan, J. P.; Szymczak, N. K. Testing the Push–Pull Hypothesis: Lewis Acid Augmented N₂ Activation at Iron. *J. Am. Chem. Soc.* **2017**, *139* (16), 5952–5956.
- (58) Kittel, C. *Introduction to Solid State Physics*, 8th ed.; Wiley: Hoboken, NJ p 20.
- (59) Que, L., Jr. *Physical Methods in Bioinorganic Chemistry: Spectroscopy and Magnetism*; University Science Books: Sausalito, CA, 2000.
- (60) Evans, D. F. 400. The Determination of the Paramagnetic Susceptibility of Substances in Solution by Nuclear Magnetic Resonance. *J. Chem. Soc.* **1959**, 2003–2005.
- (61) Schneider, C.; Guggolz, L.; Werncke, C. G. High-Spin Carbonyl Complexes of Iron(I) and Cobalt(I). *Dalton Trans.* **2021**, *51* (1), 179–184.
- (62) Geri, J. B.; Shanahan, J. P.; Szymczak, N. K. Testing the Push–Pull Hypothesis: Lewis Acid Augmented N₂ Activation at Iron. *J. Am. Chem. Soc.* **2017**, *139* (16), 5952–5956.
- (63) Eaton, M. C.; Catalano, V. J.; Shearer, J.; Murray, L. J. Dinitrogen Insertion and Cleavage by a Metal–Metal Bonded Tricobalt(I) Cluster. *J. Am. Chem. Soc.* **2021**, *143* (15), 5649–5653.
- (64) Pavão, A. C.; Taft, C. A.; Guimarães, T. C. F.; Leão, M. B. C.; Mohallem, J. R.; Lester, W. A. Interdisciplinary Applications of Pauling’s Metallic Orbital and Unsynchronized Resonance to Problems of Modern Physical Chemistry: Conductivity, Magnetism, Molecular Stability, Superconductivity, Catalysis, Photoconductivity, and Chemical Reactions. *J. Phys. Chem. A* **2001**, *105* (1), 5–11.
- (65) Lee, D.; Krebs, C.; Huynh, B. H.; Hendrich, M. P.; Lippard, S. J. Valence-Delocalized Diiron(II,III) Cores Supported by Carboxylate-Only Bridging Ligands. *J. Am. Chem. Soc.* **2000**, *122* (20), 5000–5001.
- (66) Fataftah, M. S.; Mercado, B. Q.; Holland, P. L. Valence Delocalization and Metal–Metal Bonding in Carbon-Bridged Mixed-Valence Iron Complexes. *Chem. - Eur. J.* **2023**, *29* (63), No. e202301962.
- (67) Hernández Sánchez, R.; Bartholomew, A. K.; Powers, T. M.; Ménard, G.; Betley, T. A. Maximizing Electron Exchange in a [Fe₃] Cluster. *J. Am. Chem. Soc.* **2016**, *138* (7), 2235–2243.
- (68) Arnett, C. H.; Bogacz, I.; Chatterjee, R.; Yano, J.; Oyala, P. H.; Agapie, T. Mixed-Valent Diiron μ-Carbyne, μ-Hydride Complexes: Implications for Nitrogenase. *J. Am. Chem. Soc.* **2020**, *142* (44), 18795–18813.
- (69) Buss, J. A.; Bailey, G. A.; Oppenheim, J.; Vandervelde, D. G.; Goddard, W. A.; Agapie, T. CO Coupling Chemistry of a Terminal Mo Carbide: Sequential Addition of Proton, Hydride, and CO Releases Ethenone. *J. Am. Chem. Soc.* **2019**, *141* (39), 15664–15674.
- (70) Shriver, D. F.; Van, G.; Berg, D.; Maurits, P.; Shriver, D. F.; Sailor, M. J. Transformations of Carbon Monoxide and Related Ligands on Metal Ensembles. *Acc. Chem. Res.* **1988**, *21*, 374–379.
- (71) Wannipurage, D. C.; Yang, E. S.; Chivington, A. D.; Fletcher, J.; Ray, D.; Yamamoto, N.; Pink, M.; Goicoechea, J. M.; Smith, J. M. A Transient Iron Carbide Generated by Cyaphide Cleavage. *J. Am. Chem. Soc.* **2024**, *146* (39), 27173–27178.